# Journal of Materials Chemistry

www.rsc.org/materials

Volume 18 | Number 24 | 28 June 2008 | Pages 2741–2856

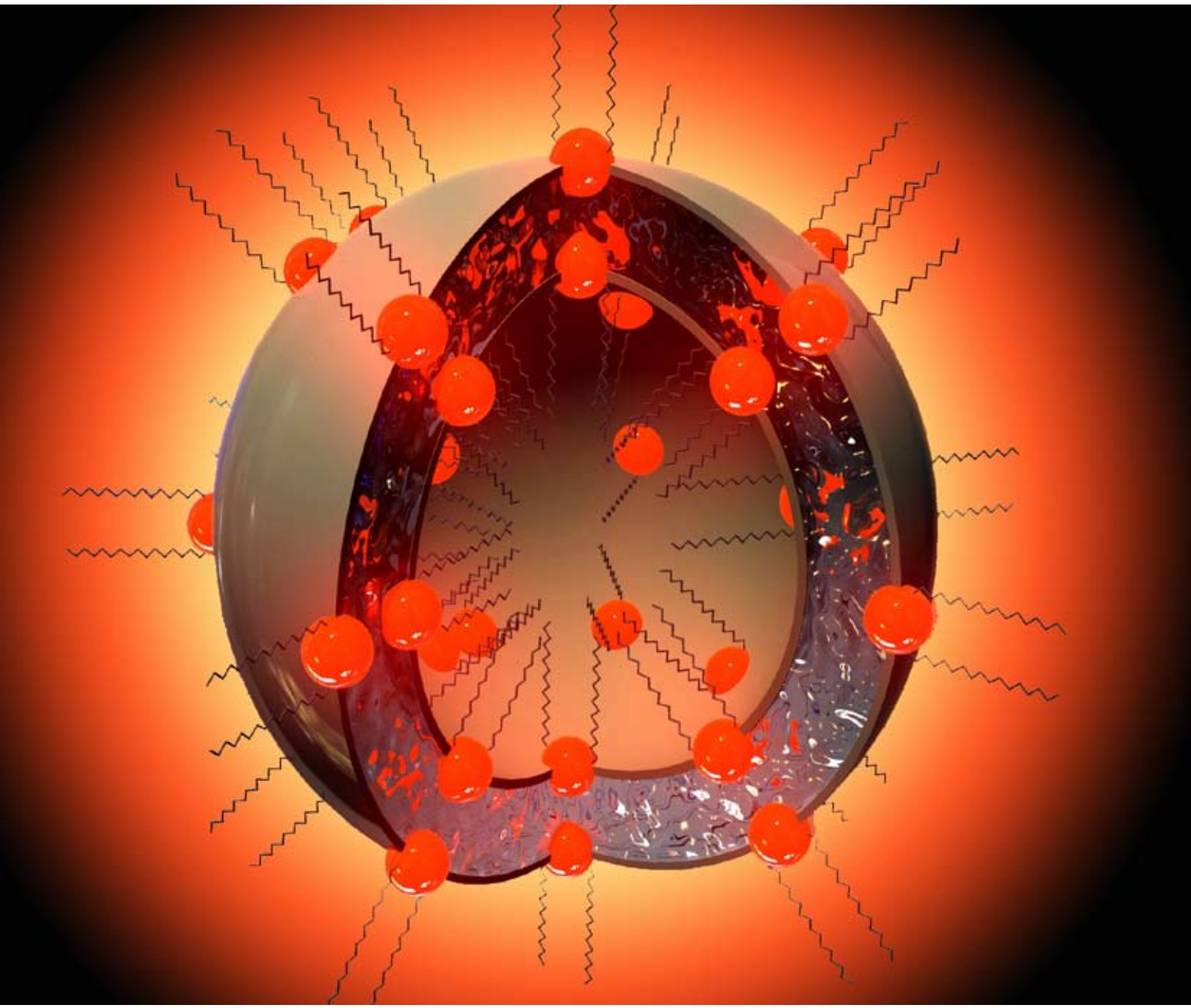

ISSN 0959-9428



RSC Publishing

0959-9428(2008)18:24;1-W

# Inverted aggregates of luminescent ruthenium metallosurfactants†

David Domínguez-Gutiérrez,[ab] Gabriele De Paoli,[b] Andrés Guerrero-Martínez,[b] Gabriella Ginocchietti,[b] Daniel Ebeling,[b] Erika Eiser,[a] Luisa De Cola*[b] and Cornelis J. Elsevier*[a]

*Received 19th November 2007, Accepted 22nd February 2008*
*First published as an Advance Article on the web 3rd April 2008*
**DOI: 10.1039/b717859j**



Metallosurfactants and their resulting aggregates combine unique spectroscopic and reactivity properties due to space confinement. We have found the requirements to obtain the first inverted micelles with luminescent metallosurfactants. The compounds possess several long linear chains that favour the solubility of the highly water-soluble metal polar head in non-polar phases. The size and shape of the aggregates have been determined using dynamic light scattering. Atomic force microscopy allowed us to study the dry structure of the aggregates on surfaces. Additionally, the self-assembly of the metal complexes in solution have been monitored by steady state and time-resolved absorption and emission spectroscopy.

## Introduction

Metallosurfactants are surface-active molecules that integrate a metal in their structure, mostly as part of the headgroup. Complexes bearing the $[Ru(bpy)^3]^{2+}$ (where bpy = 2,2′-bipyridine) unit as building block are of wide interest,[1–4] and their upgrading to surface-active molecules can improve their employment in applications such as probes in emulsions,[5,6] optoelectronics,[7] monolayers[8,9] and templates of mesoporous materials.[10–12] In fact, ruthenium-containing surfactants have already been the central subject of many studies in different areas.[13–18]

In particular, detailed studies of metallosurfactants containing $[Ru(bpy)^3]^{2+}$ as the headgroup have been performed by Bruce and co-workers.[19–22] The reported water-soluble complexes contain one alkylated bipyridine ligand that accounts for the hydrophobic part of the molecule, while the other two bipyridines are unsubstituted, conferring to the ruthenium compound with suitable counter-ions solubility in water and rendering the complex amphiphilic. Also variation in chain number, length and position of the substitution on the bpy ligand has been described.[19–23] A common characteristic among all of them is the presence of only one modified ligand that rendered water-soluble amphiphilic complexes.

An example of a metalloaggregates in a non-polar solvent has been reported by Chen and Sleiman.[24] In this case, a block copolymer can self-organise into micelles in acetonitrile–toluene mixtures, where the hydrophilic moiety is sheltered by the hydrophobic one. Apart from this study, amphiphilic complexes containing ruthenium units have solely been studied in aqueous solutions, where they aggregate into direct micelles.[17,25,26] Therefore, the role played by closely organised metal centers has not yet been explored and requires systems able to self-organise in low-polarity solvents. Inverted micelles fulfil these requirements, but to the best of our knowledge, no inverted micelles formed with metallosurfactants have been reported. From the architectural point of view, a surfactant that can aggregate into inverted micelles fulfils two key aspects: a small headgroup and voluminous hydrophobic substituents.[27] Thus, the overall shape of these molecules in the aggregates resembles a truncated cone where the headgroup represents the narrow extreme of the cone. However, related $Ru(bpy)_3^{2+}$ surfactants contain characteristically large headgroups of about 100 Å$^2$. Therefore, an indispensable prerequisite for these complexes to aggregate into inverted micelles is that the hydrophobic moieties are voluminous enough to counteract the effect inflicted by this large headgroup. Since previous studies showed that Ru-based surfactants carrying bpyR or $bpyR_2$ render spherical micelles,[20,21] we have found that the desired effect can be achieved by following two different synthetic strategies that are described in this paper. The complexes considered in this paper are of the type $[Ru(bpy)_{3-n}(bpyR_x)_n]Cl_2$, with $n = 1$ or 2 and where $bpyR_x$ stands for a 4,4′-dialkyl 2,2′-bipyridine ligand with $x$ alkyl chains. These stable complexes have properties that are easily influenced by the surrounding media, and can very well serve as models for the general design of metallosurfactants for non-polar solvents. Furthermore the full characterisation of the aggregates using different techniques, dynamic light scattering (DLS), atomic force microscopy (AFM), steady state and time-resolved absorption and emission spectroscopy is described.

## Results and discussion

### Ligand and complex synthesis

Bipyridine ligands allow a large variety of functionalisations.[28–32] Since large hydrophobic functional groups are needed in our case, we chose to employ bipyridine ligands because they easily undergo alkylation reactions. Ligand synthesis is carried out in all cases using the same procedure (see Scheme 1), except for ligand **5**. The synthesis of these ligands (**1–4**) generally proceeds

[a]*Van't Hoff Institute for Molecular Chemistry, Universitet van Amsterdam, Nieuwe Achtergracht 166, Amsterdam, 1018 WV, The Netherlands. E-mail: elsevier@science.uva.nl; Fax: +31 020/525-6456; Tel: +31 020/525-5653*
[b]*Physikalisches Institut, Westfälische Wilhems Universität Münster, Mendesltrasse 7, Münster, D-48149, Germany. E-mail: decola@uni-muenster.de; Fax: +49 0251/980-2834; Tel: +49 0251/980-2873*
† Electronic supplementary information (ESI) available: Further experimental details. See DOI: 10.1039/b717859j

 

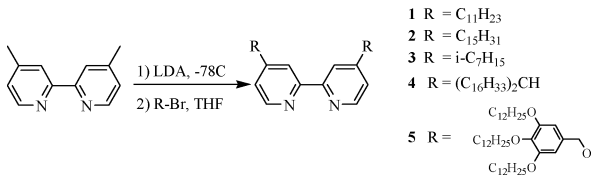


**Scheme 1** Synthesis of different 4,4′-disubstituted, 2,2′bipyridine ligands. Please note that **5** has been prepared using a different procedure (see text for details).

smoothly in good yields at low temperatures (−78 °C) using lithium diisopropylamide followed by the corresponding 1-bromoalkane while keeping the temperature low. Ligand **5** was synthesised by a simple etherification reaction in DMF using 4,4′-dihydroxy-2,2′-bipyridine and the appropriate 3,4,5-tridodecyloxybenzyl bromide. Ligands carrying linear chains can be purified by crystallisation whereas ligands with branched or more complex groups require column chromatography.

The synthetic route for the corresponding ruthenium complexes **9–11** of type $[Ru(bpy)(bpyR_2)_2]Cl_2$ is generally carried out using a stepwise synthesis. Reacting $RuCl_3$ with two equivalents of the corresponding ligand in DMF at 120 °C results in the $RuCl_2(bpyR_2)_2$ complexes **6**, **7** and **8** (Scheme 2). The use of stoichiometric amounts of ligand is crucial in order to avoid the formation of side products containing an undesired number of ligands that cause major decreases of the yields.

Complexes **6** and **7** were purified by means of size-exclusion chromatography. They display broad signals in their $^1H$ NMR spectra and their purity was assessed by elemental analyses. The second step in the procedure is the subsequent substitution of the chlorides in **6–8** by a non-modified bipyridine ligand, giving the desired complexes **9–11** with good yields (56–74%).

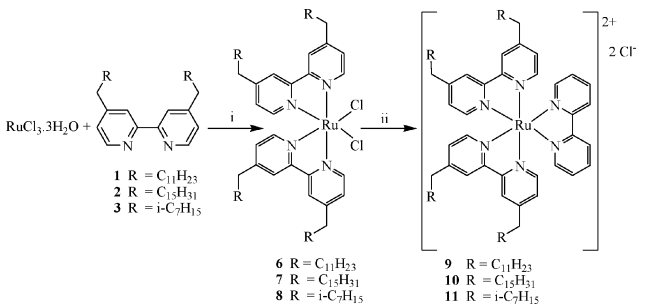


**Scheme 2** Synthesis of the metallosurfactants of type $[Ru(bpy)(bpyR_2)_2]Cl_2$ using $RuCl_3$ as precursor. i) LiCl (6 eq.), DMF, 120 °C, 16 h. ii) a) $AgNO_3$, THF, 1 h; b) 2,2′-bipyridine, THF, 60 °C, 16 h.

Procedures to achieve these products avoiding polar solvents have been described[33–35] and fortunately our $RuCl_2(bpyR_2)_2$ intermediates are well soluble in THF, where reactions proceeded smoothly. The purification of these compounds was performed by using both size-exclusion and silica gel chromatography.

In contrast to other ruthenium complexes carrying bulky groups,[36,37] complexes **12** and **13** could not be synthesised by the procedure used for **9–11**. Instead, the use of $[Ru(p\text{-cymene})Cl_2]_2$ as starting material[38–40] proved successful to synthesise products **12** and **13** (see Scheme 3). By this procedure, ligands **4** or **5** can be firstly introduced. Eventually two unmodified 2,2′-bipyridines were inserted to obtain ruthenium complexes with one large bipyridine moiety and two unmodified ones. This route results in very good yields (>70%).

## Self-aggregation

Due to the amphiphilic nature of the complex and the cone-geometry exerted by the numerous tails, it is expected that aggregation occurs in apolar solvents, leading to the formation of inverted micelles or inverted vesicles. The size and shape of the so-formed aggregates were studied by means of dynamic light scattering (DLS) and atomic force microscopy (AFM). The combination of these two complementary techniques has been successfully used in previous studies employing metallosamphiphiles.[17,25,26] DLS provides information about the hydrodynamic radius, $R_h$, of the aggregates in solution and their size distribution in different solvents, whilst AFM determines the size of the corresponding dry structures.

The results acquired in hexane and toluene solutions have been compiled in Table 1. No significant changes in the $R_h$ of the aggregates were observed over a wide range of concentrations

**Table 1** DLS data for aggregates of complexes **9–13** in apolar solvents; intensity % of the population in parentheses

| Complex | Hexane[a] | | Toluene[b] |
|---|---|---|---|
| | $R_h$ Micelles/nm | $R_h$ Vesicles/nm | $R_h$ Vesicles/nm |
| **9** | — | 64 ± 9 | — |
| **10** | 3.7 ± 0.9 (75%)[c] | 32 ± 15 (25%)[c] | 511 ± 134 |
| **11** | — | — | — |
| **12** | 3.5 ± 0.8 (32%) | 38 ± 15 (68%) | — |
| **13** | — | 49 ± 10 | 57 ± 21 |

[a] $10^{-3}$ M solutions in hexane, except for complex **10**. [b] $10^{-3}$ M solutions in toluene. [c] $5 \times 10^{-4}$ M solutions in hexane.

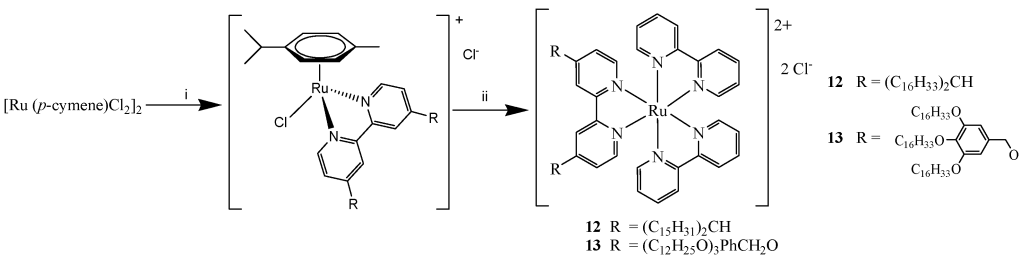


**Scheme 3** Synthesis of the metallosurfactants of type $[Ru(bpy)_2(bpyR_x)]Cl_2$ using $[Ru(p\text{-cymene})Cl_2]_2$ as precursor with ligands **4** or **5**. i) $bpyR_x$ (1 eq.), DMF, 80 °C, 6 h. ii) 2,2′-bipyridine, DMF, 120 °C, 16 h.

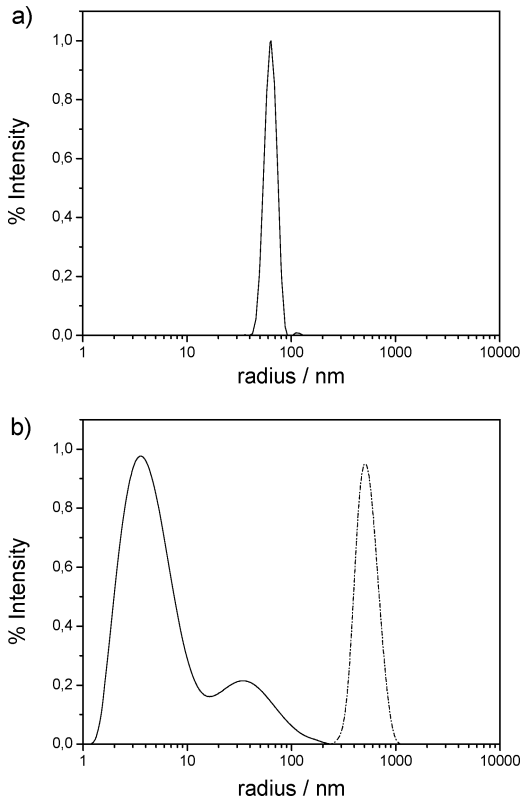


**Fig. 1** Size distribution of a) **9** in hexane and b) **10** in hexane (solid line) and toluene (dashed line).

($10^{-3}$ to $10^{-6}$ M). Additionally, no aggregates were observed when using polar solvents such as ethanol.

Complex **9** does not self-aggregate in toluene, but it forms aggregates with a hydrodynamic radius ($R_h$) of about 64 nm in hexane (Fig. 1a). Aggregates with such a large radius are vesicles and since the medium is apolar, these vesicles are inverted. The $[Ru(bpy)_3]Cl_2$ moiety is the headgroup as it has been shown in metallomicelles formed in aqueous media.[19,20,22] Inverted vesicles are formed by bilayers of complexes that close onto themselves, with the ruthenium groups facing each other. The structure of these aggregates was later studied by means of AFM in order to determine whether they simply encapsulate solvent pools or multivesciluar (onion-like) structures are formed instead.

The most remarkable aggregation results were observed for complexes **10** and **11**. The latter does not aggregate in hexane or toluene and it is not even soluble in solvents of low polarity. Despite the fact that it possesses four voluminous branched $C_9H_{19}$ chains, in principle very suitable for solubilisation in apolar solvents, it is evident that longer chains are needed to render the $[Ru(bpy)_3]^{2+}$ headgroup soluble in apolar solvents.

Interestingly, complex **10** forms inverted micelles ($R_h \approx 3.7$ nm) in $5 \times 10^{-4}$ M hexane solutions (Fig. 1b). On the other hand, $10^{-3}$ M solutions in toluene display the formation of larger structures (the radius is 100 times larger) attributed to inverted vesicles of about 500 nm radius. The large differences in aggregates' sizes are due to the polarity of the solvents; a more polar solvent such as toluene easily penetrates the interface of the surfactant, which results in larger structures. Remarkably, while **9** does not aggregate in toluene, **10** forms inverted vesicles. This different behaviour illustrates the subtle equilibrium that surfactants undergo in solution; despite sharing the same architecture as **10**, the shorter chains of **9** are responsible for a significant change in the resulting morphology of the aggregates.

The small aggregates observed for compound **10** are, to the best of our knowledge, the first inverted micelles formed by metallosurfactants. When complex **10** is dissolved in hexane, two different kind of populations are observed: a major one constituted by small aggregates, individual micelles with a $R_h$ of 3.7 nm (complex **10** with fully extended chains is estimated to have a length of 3 nm). In these small inverted micelles, the divalent ruthenium headgroups are in close contact with each other, constituting the core of the micelles, whilst the tails extend outwards to form the surface of these micelles. Alternatively, a minor population results from the coalescence of several individual micelles that would lead to larger aggregates with a mean $R_h$ of 32 nm. All aggregates formed by **10** in solution are spherical.

Complex **12** aggregates exclusively in hexane solutions. When it is dissolved in toluene, stable homogenous solutions are obtained for about 24 h, afterwards the complex precipitates. Thus, complex **12** was only measured in hexane. In this case, the aggregates are spherical and according to the size distribution results retrieved from DLS, they are monodisperse. These aggregates are inverted vesicles with a hydrodynamic radius of about 38 nm. A size distribution histogram based on DLS results shows the presence of an additional peak at low radii, which can be attributed to the formation of small aggregates (Fig. 2a). The mean position of this peak (3.5 nm) corresponds very well to the

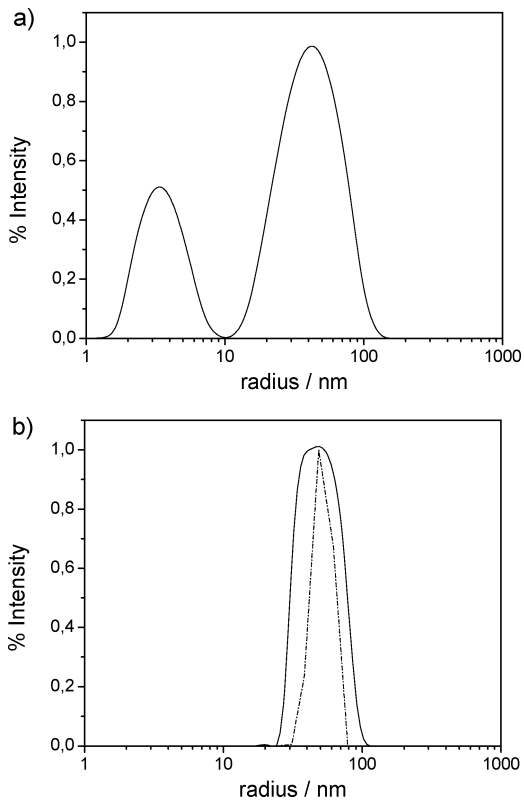


**Fig. 2** Size distributions of a) **12** in hexane and b) **13** in hexane (dashed line) and toluene (solid line).

formation of inverted micelles in hexane by **10**. Unlike complex **10**, micelles formed by **12** are however formed in a lower ratio (*ca*. 1 : 2) compared to the vesicles.

Similarly to **10**, complex **13** aggregates in hexane and toluene. The variety of aggregates formed under various conditions stems from the flexibility of ligand **5**. The aggregates are inverted vesicles, with sizes of similar orders of magnitude, with a $R_h$ of 49 nm in hexane and 57 nm in toluene. Complex **10** formed aggregates of larger radius in toluene solutions compared to those in hexane. Likewise, solutions of **13** in toluene show particles with slightly larger radii than those formed in hexane (Fig. 2b). The flexibility of the chains in ligand **5** accounts for a good adaptability of the complex to both environments regardless of the solvent influence. When comparing **13** and **12**, since both carry only one modified bpy ligand, one sees that the more rigid nature of ligand **4** causes a dramatic change in the aggregation. Thus, **12** aggregates in hexane but not in toluene (Table 1).

More information and confirmations about the aggregates can be obtained by AFM measurements. However one has to keep in mind that disagreement between AFM and DLS for the determination of the radius can been found,[18,41,42] and it is attributed to the fact that DLS determines the hydrodynamic radius while solid AFM provides the radius of the collapsed dry aggregates. For this reason, AFM images help to verify whether the inverted vesicles are indeed hollow or multivesicular (onion-like) structures, an aspect that cannot be revealed by DLS.

We have performed AFM experiments using mica as substrate and the results confirm that complex **10** forms aggregates in toluene and hexane solutions (Fig. 3). Their dimensions are similar to those obtained with DLS and yet, their height depends on the number of monomers forming the aggregates, providing insight about their structure. The larger and more robust inverted vesicles formed in toluene are higher than the more fragile inverted micelles or vesicles deposited from hexane solutions. DLS measurements clearly suggest that the vesicles objects are not in the collapsed state; the collapsed spheres would otherwise be sufficiently denser than the surrounding solvent, leading to a directed sedimentation. In that case, the behaviour would be ballistic rather than diffusive.

The analysis of the vesicles formed by **10** in toluene has been previously reported by us,[43] but not the one of the inverted micelles in hexane. The inverted micelles are small and therefore formed by a low number of monomers. According to DLS they are spherical, a feature confirmed by AFM. The second minor population seen in hexane is constituted by larger aggregates ($R_h$ ~32 nm), which can be either vesicles or coalescent micelles. Their dimensions have been confirmed by AFM measurements and the aggregates have a diameter of about 75 nm, in the range predicted by DLS. The AFM height contrast images obtained (Fig. 3) exemplify that the ratio (with respect to population) between inverted micelles and larger aggregates is in fact 3 : 1. Unfortunately, the inverted micelles have sizes that are too small to be accurately analysed with our AFM, but their sizes are in the few nanometres expected range. The large aggregate has a height of ~3 nm, in good agreement with the length of **10** with its chains totally extended. Therefore, we suppose that the aggregates are spread on the mica surface, laying flat in monolayers and not in bilayers, which is probably due to the fragility of these small structures and to the strong interaction between the highly hydrophilic mica surface and the ionic headgroup. Since special care was taken to work under non-invasive conditions, we can be sure that the measured thickness is the true thickness of the deposited particles.

Complex **9** has 16 methylene groups per molecule less than **10**. This difference has an important influence on the aggregation process as is clearly seen in the structures formed with respect to complex **10**. Apparently, the shorter chains cannot provide an efficient shielding of the headgroup in hexane solutions, rendering structures of larger curvature such as inverted vesicles instead of inverted micelles. Furthermore, the chains are too short to provide the molecule with enough amphiphilicity so it cannot aggregate in the slightly more polar toluene solutions. AFM images (see Fig. 4) show a large variety of aggregates with different sizes. We argue that the largest aggregates seen are formed due to coalescence of smaller ones upon solvent evaporation. Only the smallest ones are representative of those in solution, otherwise DLS would have provided totally different size distributions. Since DLS is very sensitive to larger particles, it is evident that the big structures seen with AFM are not the same ones in solution, but were formed during sample preparation. The thickness of the deposited particles can be measured by taking the cross-section of the individual ones, obtaining values between 12 and 14.5 nm. This thickness reinforces the idea of complex **9** forming unilamellar vesicles that result in double bilayers upon solvent evaporation.

Compound **12** forms vesicles of ~38 nm radius in apolar solvent such as hexane. The structures are not stable in more polar solvents such as toluene. These findings can be ascribed to the rigidity of the ligand; the chains are in principle long enough but not sufficient flexible to shield the headgroup. Furthermore, this rigidity hinders packing into small inverted micelles even though its general architecture would favour the fitting in

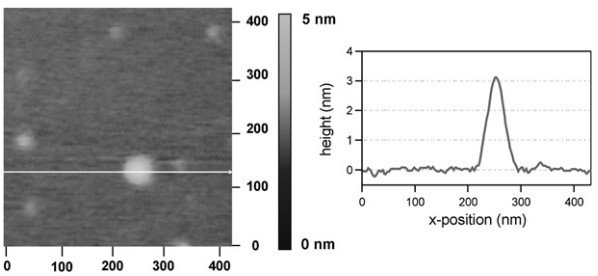


**Fig. 3** AFM height contrast image of **10** on mica upon hexane evaporation.

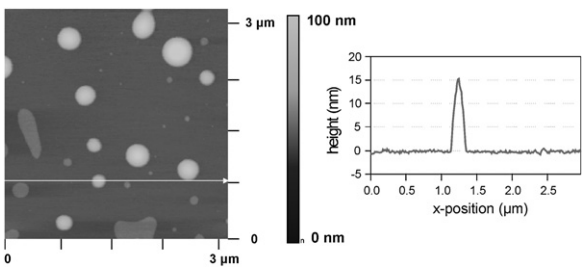


**Fig. 4** AFM height contrast image of dry aggregates of **9** on mica upon hexane evaporation.

micellar architectures. Compound **13**, as complexes **9** and **12**, forms micellar films of round aggregates, with shape and sizes determined by AFM measurements in good agreement with the DLS results.

### Photophysical characterisation

In order to compare the properties of the metallosurfactants in the presence and absence of aggregates, we studied their photophysical behavior in air-equilibrated hexane and ethanol solutions. The absorption and emission spectra of all the complexes in both solvents resemble the characteristic spectra of the $Ru(bpy)_3^{2+}$.[44] No significant differences were observed in the shape of the bands upon changing the concentration of the surfactants between $10^{-6}$–$10^{-3}$ M. Fig. 5a displays the absorption profiles in ethanol and hexane for the compound **10**. The intense band in the UV region can be assigned to the $\pi$–$\pi^*$ ligand-centered transitions ($^1$LC) localised in the bipyridine chelates. The broad band in the 420–550 nm region is due to the singlet, spin-allowed metal-to-ligand charge-transfer transitions ($^1$MLCT).

A slight bathochromic shift of the MLCT absorption and emission bands on going from apolar to polar solvents is generally expected. This phenomenon is explained in terms of the stabilisation of these polar excited states in polar media.[45] In contrast we observed a small red-shift for both absorption bands in hexane compared to the ethanol solutions, an effect that is even more pronounced for the $^1$MLCT state (Table 2). We believe that this is related with the formation of micelles and vesicles in the less polar solvent. In fact the presence of close packed Ru(II) complexes increase the polarity of the local environment inside the aggregate core reversing the effect of the solvent.[46]

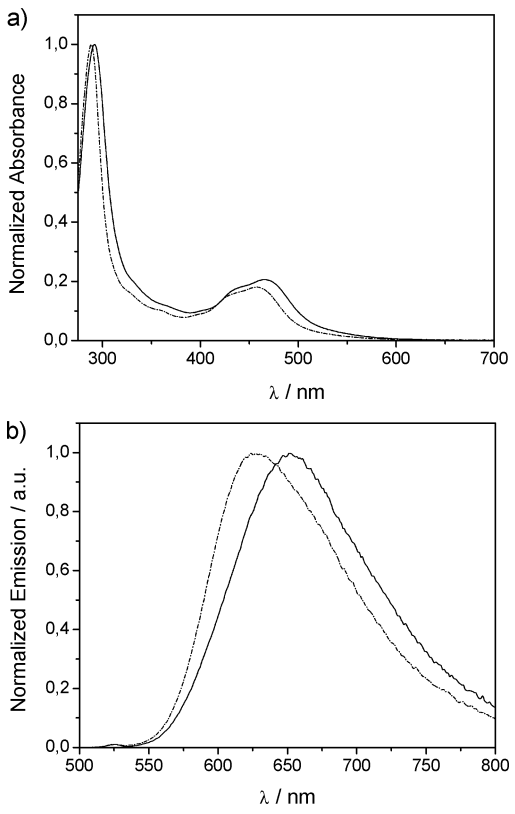


**Fig. 5** Room temperature absorption (a) and normalised emission spectra (b) of **10** in ethanol (dotted line,- - -) and in hexane (solid line,—).

**Table 2** Absorption ($\lambda_{abs}$) and emission ($\lambda_{em}$) maxima of ruthenium complexes in hexane and ethanol[a]

| | Hexane | | Ethanol | |
|---|---|---|---|---|
| Complex | $\lambda_{abs}$/nm | $\lambda_{em}$/nm | $\lambda_{abs}$/nm | $\lambda_{em}$/nm |
| **9** | 291, 462 | 642 | 288, 454 | 623 |
| **10** | 291, 464 | 651 | 288, 458 | 624 |
| **11** | — | — | 288, 460 | 625 |
| **12** | 291, 462 | 644 | 288, 454 | 623 |
| **13** | 284, 473 | 693 | 282, 483 | 687 |

[a] Emission corrected for instrument and detector response.

Luminescent spectra of compound **10** in both solvents are depicted in Fig. 5b, in which the characteristic $^3$MLCT transition from the excited state of the $Ru(bpy)_3^{2+}$ can be noticed. By examining the maxima data (Table 2), an evident red shift was observed for all the compounds in hexane, although ethanol is more polar and should stabilise the excited state more efficiently. This fact is in good agreement with the absorption results (see above).

Further evidence of the formation of aggregates was obtained by time-resolved emission spectroscopy. The excited state lifetimes of the complexes were investigated both in hexane and in ethanol. It is interesting to note that there is a great degree of scatter for the hexane time profile that corroborates the presence of micelles or vesicles.

Biexponential kinetics were found in hexane for all the compounds (Table 3). The long component is attributed to the monomeric non-aggregated ruthenium surfactants, while the short component would belong to the ruthenium moieties forming aggregates. In these systems the emission is quenched by the presence of close-packed ruthenium complexes, (triplet–triplet annihilation) which quickly reduces the luminescent excited state population.

Conversely, ethanol solutions showed monoexponential decays that correspond with only one emissive species. Furthermore it should be pointed out that the above described behavior does not depend on the excitation and emission wavelength. To definitely prove that the short component is due to the aggregation we added a drop of ethanol into the hexane samples in order to break the formation of the aggregates. The biexponential decays resulted in a single lifetime (Fig. 6, as example for

**Table 3** Emission lifetimes ($\tau$) of ruthenium complexes in hexane and ethanol.[a] $\lambda_{exc} = 431$ nm

| Complex | Hexane $\tau$/ns | Ethanol $\tau$/ns |
|---|---|---|
| **9** | 95 (16%), 413 (84%) | 195 |
| **10** | 82 (20%), 413 (77%) | 210 |
| **11** | — | 217 |
| **12** | 55 (13%), 331 (87%) | 205 |

[a] Air-equilibrated solutions.

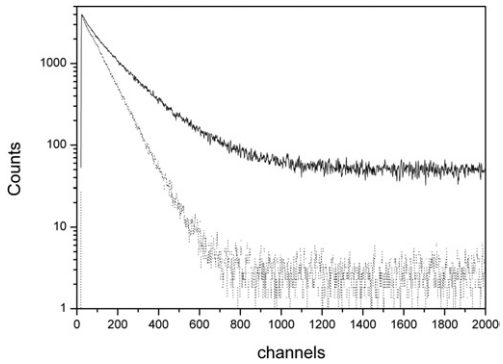


**Fig. 6** Room temperature time-resolved emission decays of complex **12** in hexane (solid line, —) and upon addition of one drop of ethanol (dotted line,- - -). Emission was monitored at 644 nm and 623 nm, respectively.

complex **12**). The different excited state lifetime in the two solvents (Table 3) are of course due to the different content of dioxygen present in ethanol *vs.* hexane.

## Conclusions

Metallosurfactants **9–13** bear the $[Ru(bpy)_3]^{2+}$ unit as a headgroup. Calculations assign a rather large headgroup area (~100 $Å^2$) to this type of metallosurfactants and yet they have proven capable of self-aggregating in aqueous solutions. As expected for packing restrictions, direct micelles are instead favoured in those cases, unless a large aliphatic part is used to counteract the effect created by the large head. Hence, if the goal is to generate inverted micelles where monomers possess such a large headgroup, a bipyridine with a large aliphatic moiety or at least two modified alkylbipyridines would be needed in order to create the desired effect whilst the complex retains its cone-shaped geometry. DLS shows that the aggregates morphology changes with the monomer employed and the solvent. The effect of the solvent is not considered in aqueous solutions, but it is a factor that dramatically influences the final architecture of inverted aggregates. The flexible nature of some of the species can be easily confirmed by this solvent effect; hexane forces complex **10** to pack into tighter aggregates to shelter the headgroup while the more polarisable toluene can accommodate within the monomers to create more expanded structures than expected by the packing parameter formula.

The formation of luminescent inverse self-assemblies represent novel aggregates that open new perspectives towards the synthesis of nanomaterials.

## Experimental

### General considerations

All synthetic experiments with metal complexes and bipyridine ligands were performed under an atmosphere of dry nitrogen using standard Schlenk techniques. All non-deuterated solvents, reagent grade or better were dried according to standard previous procedures under an atmosphere of nitrogen. Deuterated solvents were used as received. Commercially available reagents were used as received. Syntheses of compounds **1**, **2**, **6**, **7**, **9** and **10** was done as described elsewhere.[47] $Ru(p\text{-cymene})Cl_2]_2$ was synthesised according to a published procedure.[38] Size exclusion chromatography of apolar complexes was performed with Sephadex LH20 using the corresponding eluting mixtures. $^1H$ and $^{13}C\{1\ H\}$ NMR spectra were recorded at 300.13 and 75.48 MHz, respectively, using a Varian Unity 300 MHz spectrometer.

### Dynamic light scattering (DLS)

Measurements were carried out at 20 °C on a DLS set-up from ALV (Germany) with a wavelength ($\lambda_0$) of 632.8 nm. Angle-dependent measurements assured the purely diffusive nature of the aggregates formed. Dispersions in toluene (0.5 mM) or hexane (1 mM) or were prepared by a brief sonication (10 min at RT) of the compounds in the corresponding bifiltered solvent (2 ml). The resulting bright red solutions were filtered an additional time through a 0.2 μm filter prior to measurement. Solutions were measured immediately after filtration, except solutions in toluene that were left to stand for 24 h. prior to measurement. The intensity data were normalised using toluene as reference standard. Measurements at 70 °C were done using a Haake Phoenix II P2-C25 P thermoregulatory bath.

### Atomic force microscopy (AFM)

AFM analysis of particles formed from hexane solutions were carried out with a commercial atomic force microscope (Nano-Scope IIIa with MultiMode head, Veeco Instruments Inc., Münster, Germany). All the measurements were done in air applying the amplitude modulation mode, which is often referred to as "tapping mode" AFM. The images were taken with silicon cantilever (BS-Tap300, Budgetsensors) with a resonant frequency of about 330 kHz and a spring constant of about 40 N $m^{-1}$. Solutions were prepared analogously as for DLS measurements. 10 μl of fresh solution were deposited onto a small piece (1 × 1 cm) of fresh cleaved mica and allowed to dry for a few minutes.

## Acknowledgements

D.D.G. and C.J.E. thank NRSC-Catalysis for financial support, project number 2001–10. Also IRTG 1444 is acknowledged for support.

## References

1 V. Balzani, S. Campagna, G. Denti, A. Juris, S. Serroni and M. Venturi, *Acc. Chem. Res.*, 1998, **31**, 26–34.
2 C. Draeger, C. Bottcher, C. Messerschmidt, A. Schulz, L. Ruhlmann, U. Siggel, L. Hammarstrom, H. Berglund-Baudin and J. H. Fuhrhop, *Langmuir*, 2000, **16**, 2068–77.
3 G. L. Gaines Jr., *Inorg. Chem.*, 1980, **19**, 1710–14.
4 J. P. Sauvage, J. P. Collin, J. C. Chambron, S. Guillerez, C. Coudret, V. Balzani, F. Barigelletti, L. DeCola and L. Flamigni, *Chem. Rev.*, 1994, **94**, 993–1019.
5 J. T. Kunjappu, V. K. Kelkar and C. Manohar, *Langmuir*, 1993, **9**, 352–4.
6 J. T. Kunjappu, P. Somasundaran and N. J. Turro, *J. Phys. Chem.*, 1990, **94**, 8464–8.
7 R. Wang, Y. Liang and R. H. Schmehl, *Inorg. Chim. Acta*, 1994, **225**, 275–83.
8 G. Romualdo-Torres, B. Agricole, C. Mingotaud, S. Ravaine and P. Delhaes, *Langmuir*, 2003, **19**, 4688–93.

9 B. W. K. Chu and V. W. W. Yam, *Inorg. Chem.*, 2001, **40**, 3324–9.
10 M. J. Danks, H. B. Jervis, M. Nowotny, W. Z. Zhou, T. A. Maschmeyer and D. W. Bruce, *Catal. Lett.*, 2002, **82**, 95–8.
11 K. J. Holmberg, *Colloid Interface Sci.*, 2004, **274**, 355–64.
12 V. W. W. Yam, B. Li and N. Zhu, *Adv. Mater.*, 2002, **14**, 719–22.
13 B. Donnio, *Curr. Opin. Colloid Interface Sci.*, 2002, **7**, 371–94.
14 P. R. Andres and U. S. Schubert, *Adv. Mater.*, 2004, **16**, 1043–68.
15 J. D. Holbrey, G. J. T. Tiddy and D. W. Bruce, *J. Chem. Soc., Dalton Trans.*, 1995, 1769–74.
16 H. B. Jervis, M. E. Raimondi, R. Raja, T. Maschmeyer, J. M. Seddon and D. W. Bruce, *Chem. Commun.*, 1999, 2031–2.
17 G. Mayer, V. Vogel, B. G. G. Lohmeijer, J. F. Gohy, J. A. Van Den Broek, W. Haase, U. S. Schubert and D. Schubert, *J. Pol. Sci. PartA Polym. Chem.*, 2004, **42**, 4458–65.
18 J. F. Gohy, B. G. G. Lohmeijer and U. S. Schubert, *Macromol. Rapid Commun.*, 2002, **23**, 555–60.
19 J. Bowers, K. E. Amos, D. W. Bruce and R. K. Heenan, *Langmuir*, 2005, **21**, 5696–06.
20 J. Bowers, K. E. Amos, D. W. Bruce and J. R. P. Webster, *Langmuir*, 2005, **21**, 1346–53.
21 J. Bowers, K. E. Amos and D. W. Bruce, *Langmuir*, 2003, **19**, 292–8.
22 J. Bowers, K. E. Amos, D. W. Bruce and J. R. P. Webster, *Langmuir*, 2003, **19**, 299–305.
23 P. Garcia, J. Marques, E. Pereira, P. Gameiro, R. Salema and B. de Castro, *Chem. Commun.*, 2001, 1298–9.
24 B. Z. Chen and H. F. Sleiman, *Macromolecules*, 2004, **37**, 5866–72.
25 O. Regev, J. F. Gohy, B. G. G. Lohmeijer, S. K. Varshney, D. H. W. Hubert, P. M. Frederik and U. S. Schubert, *Colloid Polym. Sci.*, 2004, **282**, 407–11.
26 B. Z. Chen, K. Metera and H. F. Sleiman, *Macromolecules*, 2005, **38**, 1084–90.
27 J. N. Israelachvili, *Intermolecular and Surface Forces*, Academic Press. New York, 1992, ch. 17.
28 C. Janiak, S. Deblon, H. P. Wu, M. J. Kolm, P. Klufers, H. Piotrowski and P. Mayer, *Eur. J. Inorg. Chem.*, 1999, 1507–21.
29 S. A. Savage, A. P. Smith and C. L. Fraser, *J. Org. Chem.*, 1998, **63**, 10048–51.
30 P. D. Leeson and J. C. Emmett, *J. Chem. Soc., Perkin Trans. 1*, 1988, 3085–96.
31 P. B. Hitchcock, K. R. Seddon, J. E. Turp, Y. Z. Yousif, J. A. Zora, E. C. Constable and O. Wernberg, *J. Chem. Soc., Dalton Trans.*, 1988, 1837–42.
32 F. Blau, *Ber. Dtsch. Chem. Ges.*, 1888, **21**, 1077.
33 J. A. Connor, T. J. Meyer and B. P. Sullivan, *Inorg. Chem.*, 1979, **18**, 1388–94.
34 S. Gould, G. F. Strouse, T. J. Meyer and B. P. Sullivan, *Inorg. Chem.*, 1991, **30**, 2942–9.
35 D. P. Rillema, C. B. Blanton, R. J. Shaver, D. C. Jackman, M. Boldaji, S. Bundy, L. A. Worl and T. J. Meyer, *Inorg. Chem.*, 1992, **31**, 1600–6.
36 P. D. Beer, F. Szemes, P. Passaniti and M. Maestri, *Inorg. Chem.*, 2004, **43**, 3965–75.
37 V. Schild, D. van Loyen, H. Durr, H. Bouas-Laurent, C. Turro, M. Worner, M. R. Pokhrel and S. H. Bossmann, *J. Phys. Chem.*, 2002, **106**, 9149–58.
38 M. A. Bennett, T. N. Huang, T. W. Matheson and A. K. Smith, *Inorg. Synth.*, 1982, **21**, 75.
39 R. Drozdzak, B. Allaert, N. Ledoux, I. Dragutan, V. Dragutan and F. Verpoort, *Coord. Chem. Rev.*, 2005, **249**, 3055–74.
40 C. Klein, K. Nazeeruddin, D. Di Censo, P. Liska and M. Gratzel, *Inorg. Chem.*, 2004, **43**, 4216–26.
41 J. F. Gohy, H. Hofmeier, A. Alexeev and U. S. Schubert, *Macromol. Chem. Phys.*, 2003, **204**, 1524–30.
42 J. F. Gohy, B. G. G. Lohmeijer, S. K. Varshney and U. S. Schubert, *Macromolecules*, 2002, **35**, 7427–35.
43 D. Dominguez-Gutierrez, M. Surtchev, E. Eiser and C. J. Elsevier, *Nano Lett.*, 2006, **6**, 145–7.
44 A. Juris, V. Balzani, F. Barigelletti, S. Campagna, P. Belser and A. Von Zelewsky, *Coord. Chem. Rev.*, 1988, **84**, 85–277.
45 E. M. Kober, B. P. Sullivan and T. J. Meyer, *Inorg. Chem.*, 1984, **23**, 2098–2104.
46 P. K. Gosh and A. J. Bard, *J. Phys. Chem.*, 1984, **88**, 5519–26.
47 D. K. Ellison and R. T. Iwamoto, *Tetrahedron Lett.*, 1983, **24**, 31–2.


 